Final Report

Project Title: Energetics of native defects in anatase TiO_2: A hybrid density functional study

By : Dr. Adisak Boonchun

Contract No. TRG5780264 :

Contract No. TRG5780264 :

Final Report

Energetics of native defects in anatase TiO_2: A hybrid density functional study

Adisak Boonchun
Kasetsart University

Project Granted by the Thailand Research Fund Office of the Higher Education Commission and Kasetsart University

Project Code : TRG5780264

Project Title : Energetics of native defects in anatase TiO_2: A hybrid density functional study

Investigator : ADISAK BOONCHUN

E-mail Address : nanodsci@gmail.com

Project Period : 15 July 2014 - 14 July 2016

Abstract

The energetics and electronic structures of native defects in anatase TiO_2 are comprehensively studied using hybrid density functional calculations. We demonstrate that oxygen vacancies (V_O) and titanium interstitials (Ti_i) act as shallow donors, and can form with substantial concentrations, giving rise to free electrons with carrier densities from 10^{11} to 10^{19} cm^{-3} for oxygen-rich and oxygen-poor conditions, respectively. The titanium vacancies (V_{Ti}), identified as deep acceptors and induced hole carriers, are incapable of fully compensating for the free electrons originating from the donor-type defects at any oxygen chemical potential. Even under an extreme oxygen-rich condition, the Fermi level, which is determined from the charge neutrality condition among charge defects, electron and hole carriers are located 2.34 eV above the valence band maximum, indicating that p-type conductivity can never be realized under any growth conditions without external doping. This is consistent with common observations of intrinsic n-type conductivity of TiO_2. At a typical annealing temperature and under a typical oxygen partial pressure, the carrier concentration is found to be approximately 5×10^{13} cm^{-3}.

keywords: Density Functional Theory, anatase TiO_2, native defect, defect calculation

รหัสโครงการ : TRG5780264

ชื่อโครงการ: การศึกษาพลังงานในการเกิดความบกพร่องผลึกของไทเทเนียมไดออกไซด์ โดยใช้ทฤษฎีพังก์ชันนัลของความหนาแน่นแบบไฮบริด

ผู้วิจัยหลัก: ผศ.ดร. อดิศักดิ์ บุญชื่น

อีเมล์ : fsciasb@ku.ac.th

ระยะเวลาโครงการ : เริ่มตั้งแต่ 15 กรกฎาคม 2014 ถึง 14 กรกฎาคม 2016

บทคัดย่อ: พลังงานและโครงสร้างทางอิเล็กทรอนิคของความบกพร่องผลึกในไททาเนียมไอออกไซด์ (TiO_2) แบบอนาเทส (anatase) ได้ถูกศึกษาโดยใช้ทฤษฎีพังก์ชันนัลของความหนาแน่นแบบไฮบริด, การวิจัยพบว่าการหายไปของออกซิเจน (V_O) และการแทรกของไททาเนียม (Ti_i) จะเกิดระดับพลังงานผู้ให้แบบตื้น (shallow donors) ซึ่งเป็นผลให้ค่าความหนาแน่นอิเล็กตรอนอิสระมีค่ามาก ประมาณ 10^{11} และ 10^{19} อิเล็กตรอนต่อลูกบาศก์เซ็นติเมตร. ในสถาวะออกซิเจนมากและ ออกซิเจนน้อย ตามลำดับ สำหรับการหายไปของไทเทเนียนม จะให้ระดับพลังงานผู้รับแบบลึก (deep acceptor) ซึ่งทำให้เกิดพาหะโฮล โดยไม่สามารถจับกับอิเล็กตรอนอิสระในสภาวะการปลุกผลึกแบบต่างๆ ในสภาวะปลูกผลึกที่เต็มไปด้วยออกซิเจน ระดับพลังงานเฟอร์มีซึ่งหาได้จากสถาพความเป็นกลางของประจุผลึก ของผลึกที่มีความบกพร่อง ระดับพลังงานเฟอร์มีถูกตรึงไว้ที่ระดับ 2.34 อิเล็กตรอนโวลท์ เหนือแถบพลังงานวาเลนซ์สูงสุด จึงสรุปได้ว่า สารกึ่งตัวนำของ ไม่สามารถเกิดเป็นชนิดพีได้ ภายใต้การปลูกผลึกใต้สภาวะใดๆ เมื่อไม่ได้มีสารเจือ งานวิจัยนี้สอดคล้องกับการพบการนำไฟฟ้าชนิดเอ็น ของสารไทเทเนียมไดออกไซด์ นอกจากนี้พบว่าภายในการปลูกผลึกสภาวะปกติ ความหนาแน่นภาหะมีค่าประมาณ 5×10^{13} อิเล็กตรอนต่อลูกบาศก์เซ็นติเมตร.

1 Abstract

The energetics and electronic structures of native defects in anatase TiO_2 are comprehensively studied using hybrid density functional calculations. We demonstrate that oxygen vacancies (V_O) and titanium interstitials (Ti_i) act as shallow donors, and can form with substantial concentrations, giving rise to free electrons with carrier densities from 10^{11} to 10^{19} cm^{-3} for oxygen-rich and oxygen-poor conditions, respectively. The titanium vacancies (V_{Ti}), identified as deep acceptors and induced hole carriers, are incapable of fully compensating for the free electrons originating from the donor-type defects at any oxygen chemical potential. Even under an extreme oxygen-rich condition, the Fermi level, which is determined from the charge neutrality condition among charge defects, electron and hole carriers are located 2.34 eV above the valence band maximum, indicating that p-type conductivity can never be realized under any growth conditions without external doping. This is consistent with common observations of intrinsic n-type conductivity of TiO_2. At a typical annealing temperature and under a typical oxygen partial pressure, the carrier concentration is found to be approximately 5×10^{13} cm^{-3}.

2 Executive Summary

Introduction and Literature review

TiO_2 is a technologically important wide-bandgap semiconductor with applications as a transparent conducting oxide (TCO),[17, 24] in photocatalysis,[16] solar cells[19, 1] and as a ferromagnetic wide-bandgap oxide.[40, 59] TiO_2 exists as three polymorphs: rutile, anatase, and brookite. Anatase has been a favored phase for nanopowdered photocatalytic applications due to its higher activity than rutile[50, 56], although nanostructures like nanorods and nanotubes with rutile structure have also been synthesized.[36, 6] Anatase phase is important for TCO applications possibly due to its smaller electron-effective mass than rutile. There are several reports on doping for n-type conductivity of anatase TiO_2-based TCO,[17, 52, 15, 18, 23] reports on p-type conductivity are very rare. The photoexcitation of electron-hole pairs in pristine TiO_2 requires relatively high photon energy and occurs only under ultraviolet light. In practice, reduced TiO_2 can absorb photon in visible light region according to the abundance of trivalent Ti (Ti^{3+}).[25, 11] Reduced TiO_2 also exhibits n-type conductivity,[12, 2, 43] the origin of which was proposed to be donor-type defects like oxygen vacancies (V_O) and titanium interstitials (Ti_i).[12] First-principles cal-

culations based on density functional theory (DFT) have been established as an important tool for understanding and acquiring knowledge of native defects in general.

Native defects in anatase TiO_2 were previously studied using local-density approximation (LDA) and generalized gradient approximation (GGA).[42, 45] However, recent studies revealed that self-interaction correction and its repercussions for polaronic effects are important for discussing electronic and magnetic properties of native defects in metal oxides.[30] The approximation methods that include some of the essential correlation- or orbital-dependent effects, such as LDA+U (or GGA+U) and hybrid functionals, are more insightful for understanding of and gaining knowledge about native defects. Morgan and Watson[41] reported a GGA+U study of the transition levels and single-particle levels of donor- and acceptor-type native defects in anatase TiO_2. They suggested that V_{O} and Ti_i are deep donors that donate two and four electrons, respectively, whereas V_{Ti} are deep acceptors generating four holes.

Since Heyd-Scuseria-Ernzerhof (HSE) hybrid functional[21] yields a better description of bandgap, it should also be useful for accurate estimations of the defect levels in semiconductors and metal oxides. Janotti *et al.*[27] performed HSE hybrid functional calculations on rutile TiO_2 and showed that oxygen vacancies are stable in their positively charged states V_{O}^{2+} for any Fermi energy within the bandgap, indicating that they are shallow donors. Recently, P. Deák *et al.*[9] also studied oxygen vacancies and carrier self-trapping in anatase and rutile TiO_2 using HSE06,[21] and showed that oxygen vacancies are shallow donors in both anatase and rutile phases. Finazzi *et al.*[14] demonstrated using GGA+U (with U=4 eV) or B3LYP hybrid functional that charge-neutral oxygen vacancies in anatase TiO_2 create defect states at 1 eV below the conduction band. Recently, P. Deák *et al.*[10] found that oxygen vacancies and titanium interstitial are both shallow donors by using HSE06. The single-particle Kohn-Sham levels associated with Ti interstitials were also investigated using spin-polarized hybrid DFT.[14] Malashevich *et al.*[39] studied oxygen vacancies in rutile structure using DFT+*GW*, and found that the transition level of charged states from +2 to +1, $\varepsilon(+2/+1)$, is higher than that of +2 to neutral, $\varepsilon(+2/0)$, showing negative U behavior. From their estimation $\varepsilon(+2/0)$ lies 2.8 eV above the VBM.

These theoretical studies mainly focused on the identification of defect levels and the validation of computational results obtained from the different methods. However the Fermi

level position and carrier concentrations in intrinsic anatase TiO_2 have not been quantitatively estimated. Moreover, the origin of the n-type conductivity is still controversial and a theoretical study based on accurate computational methods is required.

Objective

In this study, we employ the HSE06 hybrid functional, which was proven to be reliable for defect calculations in TiO_2,[8] to conduct a comprehensive study for the energetics of native defects in anatase TiO_2 and to estimate carrier concentration under a given oxygen partial pressure. Since the antisite defects (Ti_O and O_{Ti}) have high formation energies,[42] they are not considered in the present study. The native point defects examined in this study are V_{Ti}, V_O, Ti_i and O interstitials (O_i) in anatase TiO_2.

Computational method

Our study is based on DFT calculations using the HSE hybrid functional.[21] The calculations were performed using the VASP code [29] with the projector-augmented wave (PAW) method.[3] We used a well-converged energy cut-off of 400 eV for the projector-augmented plane waves. In conventional unit cells, the Brillouin zone is expressed using $5 \times 5 \times 5$ Monkhorst-Pack meshes.

For Ti, $3s^2 3p^6 4s^2 3d^2$ states were treated as valence states. In the HSE approach, the Coulomb potential in the exchange energy is divided into short-range and long-range parts with a screening length of 10 Å. In the short-range part, the non-local Hartree-Fock (HF) exchange is mixed with the Perdew, Burke, and Ernzerhof (PBE) GGA exchange energy. [46] The long-range part and the correlation potential are represented by the PBE functional.

We used the standard HF mixing $\alpha = 0.25$ which is suitable for satisfaction of the generalized Koopmans' theorem[33] in both anatase and rutile TiO_2 [8]. The geometry relaxation was performed for a cell volume and shape, as well as for atomic positions of 12-atom conventional cell, until the residual force is less than 0.02 eV/Å. Our calculated lattice constants are a=3.760 Å and c=9.621 Å, which were close to other HSE06-reported constants of a=3.755 Å and c=9.561 Å,[8] and experimental results: a=3.782 Å and c=9.502 Å.[4]

Our calculated indirect bandgap is 3.73 eV for the transition from the valence band maximum (VBM) near M point (0.425, 0.425, 0) to the conduction band minimum (CBM) at Γ. Although we attempted to use the same cut-off energy and valence electron configuration potentials as were used in previous HSE06 calculation,[8] we somehow still obtained a larger bandgap, which is accidentally equal to the adiabatic bandgap of G_0W_0 calculation (3.73 eV).[31] Note that, both HSE06 and quasi-particle G_0W_0 bandgaps are higher than the experimentally measured optical bandgap (3.42 eV)[51]

For defect calculation, we extended the conventional cell by $3\times3\times1$ to produce a 108-atom supercell and introduced a defect in the supercell. K-points were sampled at a Monkhorst-Pack special $1\times1\times1$ mesh for the Brillouin zone integration of the supercell. Calculations for charged states were also performed for each defect with neutralizing background charge. The charged states considered here are (+2, +1, 0) for V_{O}, (+4, +3, +2, +1, 0) for Ti_i, (-4, -3, -2, -1, 0) for V_{Ti} and (+2, +1, 0) for O_i. The effects of spin polarization were included for all charged states. Relaxations were performed for atomic positions with a fixed cell volume until the residual force is less than 0.02 eV/Å.

Fictitious interactions between the charged defect with its images in neighboring cells and with the homogeneous background charge were removed using the scheme proposed by Makov and Payne.[38] Normally, the quadrupole term in the Makov and Payne correction can be approximated to about one-third of the monopole term for cubic supercells as reported by Lany and Zunger.[32] Since the supercell used in this study is non-cubic, the non-cubic adjustment[28] has been used to correct the quadrupole term in Makov and Payne. The dielectric constant is needed in the Makov and Payne correction. From HSE calculations for dielectric constants of anatase TiO_2,[35] the average value of 46.23 was used in the correction.

To ensure the convergence of the cell size, especially for high-charge-state defects, we tested the formation energy calculations of oxygen vacancies in neutral charged states with a larger supercell size of 216 atoms, i.e. $3\times3\times2$ extension of the conventional cell. We found that the formation energy of neutral charge V_{O} is changed only by 0.075 eV as cell size increased from 108 to 216 atoms. The relaxed geometries for all defects examined are shown in Fig. 1

To identify the dominant type of native defect, we compared the stabilities of Ti_i, V_{Ti}, V_{O}

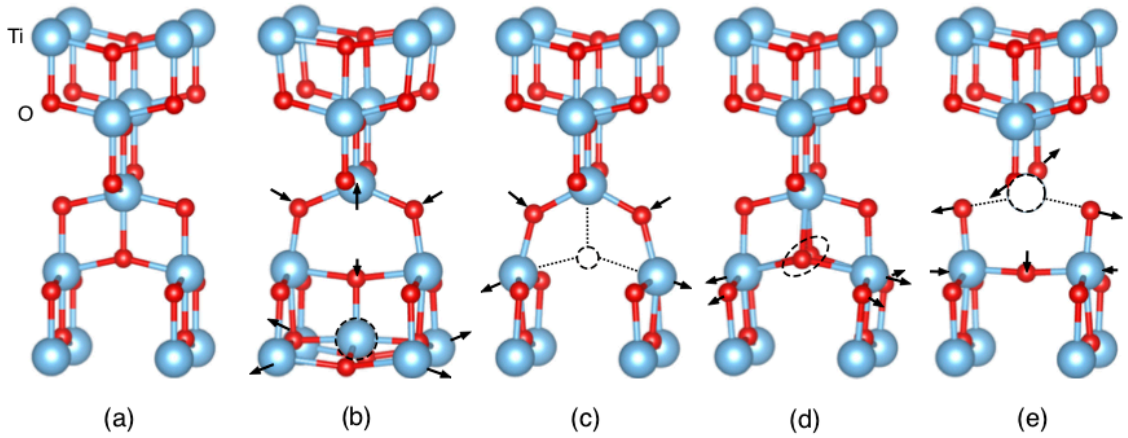

Figure 1: The optimized atomic structure of (a) bulk (b) Ti_i^{4+} (c) V_O^2 (d) $O_{i,db}$ and (e) V_{Ti}^{4-} defect. The large gray spheres are Ti atoms and the small red spheres are the O atoms. Relaxation around neighboring defect atoms are indicated by the arrows

and O_i. The formation energy of a native defect D with charge state q is defined as

$$E_f(D^q) = E_{tot}(D^q) - E_{tot}(\mathrm{TiO_2}) - \mathrm{n_i}\mu_\mathrm{i} + q(\varepsilon_\mathrm{F} + E_\mathrm{V}), \tag{1}$$

where $E_{tot}(D^q)$ is the total energy of the cell with defect D in charge state q. $E_{tot}(\mathrm{TiO_2})$ is the total energy of the cell without defects, $\mathrm{n_i}$ is the number of atoms of species i (Ti or O) that have been added to ($\mathrm{n_i} > 0$) or removed from ($\mathrm{n_i} < 0$) the supercell. ε_F is the Fermi energy that ranged over the bandgap. Note that ε_F is the energy of the electron reservoir with respect to the VBM, E_V, which is corrected in a defect-containing supercell by aligning the electrostatic potential at a region far away from the defect site with the corresponding potential in a perfect crystal.

Finally, μ_i is a chemical potential representing the energy for defect D that is taken from reservoir. We reference chemical potentials $\tilde{\mu}_i$ to the energy per atom of isolated elemental phase: $\tilde{\mu}_\mathrm{O} = \mu_\mathrm{O} - \frac{1}{2}E_{tot}[\mathrm{O_2}]$ and $\tilde{\mu}_\mathrm{Ti} = \mu_\mathrm{Ti} - E_{tot}[\mathrm{Ti}_{bulk}]$. These reference energies are given by our DFT calculations for a total energy of bulk Ti per formula unit (-9.46 eV) and a half of total energy of an isolated O_2 molecule (-8.55 eV).

The chemical potential is a variable but it must satisfy the thermodynamic equilibrium

condition of TiO_2, $\tilde{\mu}_{Ti} + 2\tilde{\mu}_O = \Delta H_f(TiO_2)$ where $\Delta H_f(TiO_2)$ is the formation enthalpy of TiO_2. At the oxygen-rich limit ($\tilde{\mu}_O$=0), the chemical potential of Ti is given by $\tilde{\mu}_{Ti} = \Delta H_f(TiO_2)$. At the Ti-rich limit, $\tilde{\mu}_{Ti}$ is bounded by the formation of Ti_2O_3, $2\tilde{\mu}_{Ti} + 3\tilde{\mu}_O < \Delta H_f(Ti_2O_3)$.[42] The formation enthalpies estimated using the HSE approach are $\Delta H_f(TiO_2)$= -9.756 eV and $\Delta H_f(Ti_2O_3)$= -15.493 eV which are in good agreement with the previous report.[55, 44] After all, the chemical potential settings ($\tilde{\mu}_{Ti}$, $\tilde{\mu}_O$) corresponding to Ti-rich (O-poor) and O-rich (Ti-poor) are (-1.72,-4.02) and (-9.76, 0) in eV, respectively.

In addition to the extreme chemical potential conditions (Ti-rich and O-rich), we consider an intermediate oxygen chemical potential corresponding to a realistic growth condition during the annealing of anatase TiO_2. The oxygen chemical potential is a function of temperature and oxygen partial pressure, as described by[47]

$$\tilde{\mu}_O(T, p) = \tilde{\mu}_O(T, p_0) + \frac{1}{2} k_B T \ln(p/p_0), \tag{2}$$

where $\tilde{\mu}_O(T, p_0)$ is the oxygen chemical potential at the standard pressure $p_0 = 1$ atm, k_B is Bolzmann's constant, and T is the temperature in Kelvin. The typical annealing temperature used in the growth of anatase TiO_2 is 400-550°C[17, 24, 26] and the typical oxygen partial pressure is 10^{-4}-10^{-5} Torr.[22] We therefore choose an annealing temperature of 550°C and an oxygen partial pressure of 10^{-5} Torr, which corresponds to ($\tilde{\mu}_{Ti}$, $\tilde{\mu}_O$) = (-6.70, -1.52) in eV.

The thermodynamic transition levels are given by the Fermi energy at which the formation energies of the two charged states are equal:

$$\varepsilon_D(q/q') = \frac{E_f(D^q; \varepsilon_F = 0) - E_f(D^{q'}; \varepsilon_F = 0)}{q' - q} \tag{3}$$

which thermodynamic transition represented by kinks in the plots of formation energy as a function of Fermi energy. Note that ε_F ranges over the bandgap and references to the VBM.

The concentration of a native defect D with charge q, c(D^q), is related to its formation

energy E_f through the equation

$$c(D^q) = N_{\text{sites}}/(1 + \exp^{E_f(D^q)/k_BT}), \tag{4}$$

where N_{sites} is the number of possible lattice sites per unit volume (V_{cell}) at which the defect can be formed.

The hole concentration (p) and electron concentration (n) can be expressed by the following equations:[20]

$$n = 2\left(\frac{m_e k_B T}{2\pi\hbar^2}\right)^{3/2} \exp^{(\varepsilon_F - \mathrm{E}_g)/k_BT}, \tag{5}$$

$$p = 2\left(\frac{m_h k_B T}{2\pi\hbar^2}\right)^{3/2} \exp^{-\varepsilon_F/k_BT}, \tag{6}$$

where m_e, m_h are the electron- and hole-effective masses, respectively, and E_g is the bandgap. The charge neutrality is satisfied when the summation of donor and electron carrier concentrations equals the acceptor and hole carrier concentrations,

$$\sum_i q_i c_i(D^q) + p - n = 0. \tag{7}$$

The index i represents donor- or acceptor-type defect. In our calculations, the experimental hole-effective mass of $0.8m_0$ and electron effective mass of $1.2m_0$ were used.[58]

3 Results

Figure. 2 shows the formation energies obtained from our hybrid DFT calculations as a function of the Fermi energy. The lower and upper limits of the Fermi energy correspond to the VBM and CBM, respectively. The slope of each line reflects the stable charged state of each defect, *e.g.* V_{O}^{2+} is stable over the other charged states of V_{O} in the entire range of Fermi energies. The transition levels $\varepsilon(q/q')$ corresponding to each defect are listed in Table. 1, some of which are also shown as filled circles in Fig. 2

Under Ti-rich conditions (Fig. 2(a)), Ti_i^{4+} has the lowest formation energy among the de-

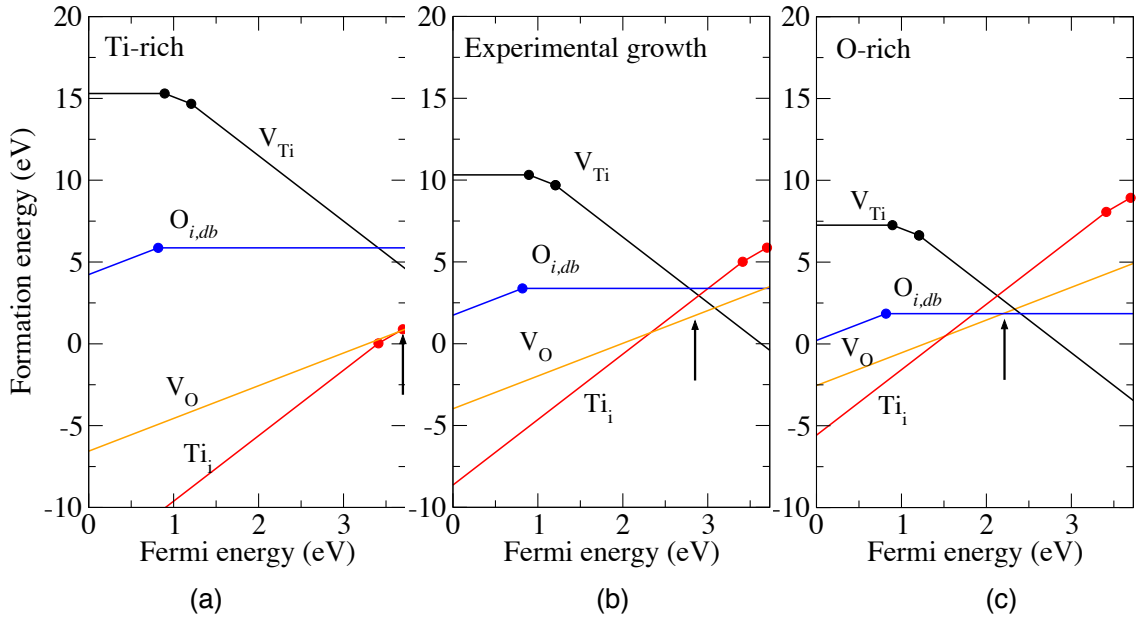

Figure 2: Defect formation energies as a function of Fermi energy under (a) Ti-rich, (b) experimental growth, and (c) O-rich conditions. The up-pointing arrow indicates the Fermi level determined by the charge neutrality condition at 550 °C.

fects examined over a wide range of Fermi energies. However, the predominance overturns at a higher Fermi energy, i.e. the formation energy of V_{O}^{2+} is slightly lower than that of Ti_i^{4+} near CBM. On the other hand, the formation energy of V_{Ti}^{4-} is higher than those of V_{O}^{2+} and Ti_i^{4+} at any Fermi level, indicating that hole carriers induced by the acceptor-type defect (V_{Ti}^{4-}) are incapable of compensating for electrons induced by the donor-type defects (V_{O}^{2+} and Ti_i^{4+}). In fact, the Fermi level determined by the charge neutrality condition under a typical annealing temperature of 550 °C is pinned at the CBM under the Ti-rich condition according to our following analysis. The pinned Fermi levels are denoted as up-pointing arrows in Fig. 1 for each $\tilde{\mu}_{\mathrm{O}}$ condition. When the transition level is above CBM, Fermi level is considered pinned at the CBM. At the oxygen-rich limit, the formation energy of V_{Ti}^{4-} is lowered and the carrier compensation effect is more pronounced, as observed in the downward shift of the Fermi level, although it is still higher than the VBM by 2.34 eV and cannot reach p-type conductivity (Fig. 2(c)). Here, the formation of V_{O}^{2+} is still favored compared to Ti_i^{4+} at the pinned Fermi level. Under an intermediate μ_{O} corresponding to an experimental growth condition (oxygen partial pressure 10^{-5} Torr at 550 °C) [22], the

Table 1: The transition level $\varepsilon(q, q')$ all in eV reference to the VBM

Defect	q, q'	$\varepsilon(q, q')$
V_{O}	+2/+	3.92
	+2/0	3.82
Ti_i	+4/+3	3.41
	+3/+2	3.70
	+2/+1	3.82
	+1/0	4.01
V_{Ti}	0/-2	0.89
	-2/-4	1.21
O_i	+2/0	0.81

Fermi level is located at 2.72 eV. Again, V_{O}^{2+} predominates over Ti_i^{4+} at the pinned Fermi level (Fig. 2(b)), and therefore is considered the major source of electron carriers. Thus, V_{O}^{2+} is the predominant donor-type defect under any $\tilde{\mu}_{\mathrm{O}}$ condition.

Ti_i is stable in the form of quadruple charged state. The nearest oxygen neighbor along the vertical c-axis relaxes inward by 23.6% in Ti_i while the two nearest-neighbor oxygen atoms on the basal axis relax outward by only 0.37%. The optimized structure of Ti_i is shown in ESI Fig. S1.(b). Most of the thermodynamic transition levels for Ti_i shown in Table I are located above the CBM, reflecting that it is a shallow donor.

V_{O} is stable in the doubly charged state. There are three nearest-neighbors Ti atoms around V_{O}. In neutral charge state, one Ti nearest-neighbor relaxes outwards by 8.39% while the other two relax outwards by 2.80%. The optimized structure of V_{O} is shown in ESI Fig. S1.(c). The transition levels $\varepsilon(+2/+)$ and $\varepsilon(+2/0)$ (not shown in Fig. 2) are located above the CBM, which is consistent with previous reports using the HSE approach for rutile[27] and antase[10]. Note that in our HSE06 calculation, we used low-frequency limit of the dielectric constant in Lany-Zunger charge correction[32] while P. Deák *et al.*[10] applied high-frequency dielectric constant in Lany-Zunger charge correction. Interestingly, our calculation and P. Deák *et al.*[10] yield qualitatively consistent results in terms of the point that both V_{O} and Ti_i exhibit the nature of shallow donors. By contrast, DFT+U predicted they are deep donors.[41, 55]

O_i atoms are more stable in dumbbell configuration ($\mathrm{O}_{i,db}$) than in an octahedral configu-

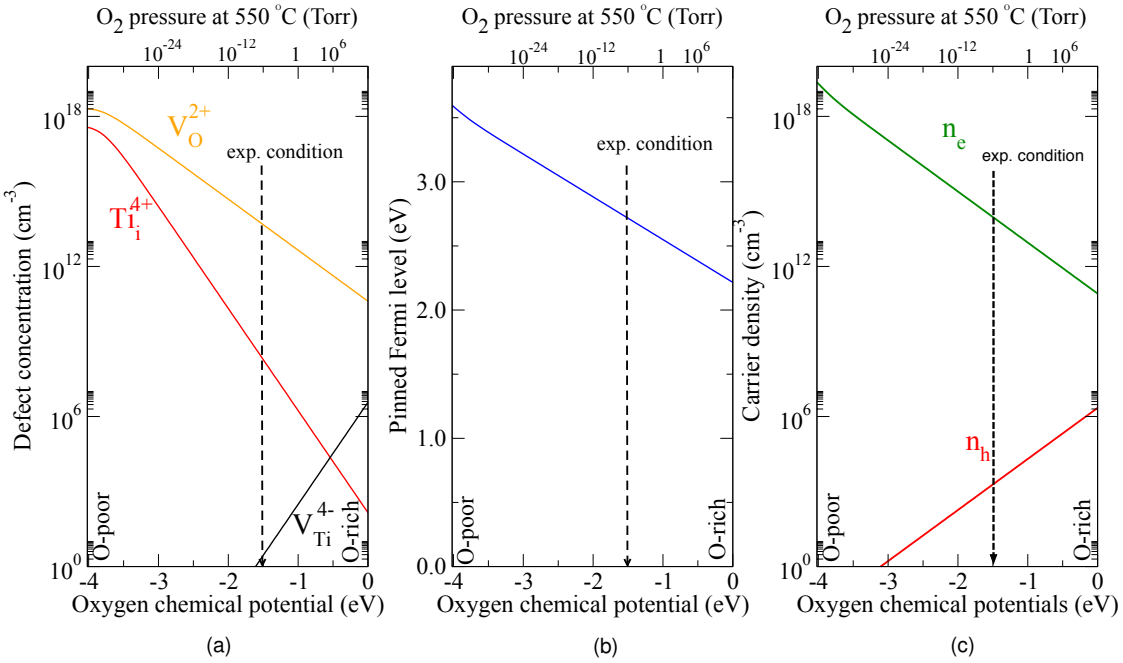

Figure 3: (a) The defect concentration (b) pinned Fermi energy and (c) carrier concentration (electrons n_e and holes n_h) as a function of oxygen chemical potentials. The down-pointing arrow with the vertical dashed line indicates the oxygen chemical potential, -1.52 eV, corresponding to the experimental condition at the annealing temperature of 550°C and under an oxygen partial pressure of 10^{-5} Torr.

ration ($O_{i,oct}$), in the form of peroxide ions at oxygen lattice sites. All the neighboring Ti atoms relax outward only slightly. The optimized structure of $O_{i,db}$ is shown in ESI Fig. S1.(d). Substitutional O_2 has a bond length of 1.44 Å in the neutral charge state, which is slightly longer than that in an isolated O_2 molecule (1.21 Å). The transition level $\varepsilon(+2/0)$ is located 0.81 eV above the VBM, indicating that it is a deep donor. The detailed analysis of O_i have been studied by Paul Erhart *et al.*[13]

V_{Ti} defect changes its charge state from neutral to -2 to -4 as the Fermi energy increases, as shown in Fig. 2. The thermodynamic transition levels are located in the band gap: $\varepsilon(0/-2)$ = 0.89 and $\varepsilon(-2/-4)$ = 1.21 eV, which indicates that V_{Ti} is a deep acceptor. Recently, Chen and Dawson show that V_{Ti} is not stable with respect to the complex defect $V_{\mathrm{Ti}} + 2V_{\mathrm{O}} + \mathrm{O}_2$ for the Fermi level less than 1.37 eV by using HSE06.[5] The formation energy of this complex is very high and does not contribute in our charge neutrality calculation. In anatase, the axial bond lengths are longer than the equatorial bond lengths. The nearest-

neighbor oxygen atoms in the basal plane containing V_{Ti}^{4-} relax outwards by 4.6%, whereas the nearest-neighbor oxygen atoms in the axial direction relax outwards by 20%. The optimized structure of V_{Ti} is shown in ESI Fig. S1.(e).

Fig. 3(a) shows defect concentrations as a function of oxygen chemical potential or oxygen partial pressure at 550°C. Note that Eq. 7 is satisfied for each oxygen chemical potential in the plots shown in Fig.3. It is clear that the concentration of V_{O}^{2+} is higher than that of $\mathrm{Ti_i^{4+}}$ for any oxygen chemical potential, while the concentration of V_{Ti}^{4-} is limited. Note that we considered only point defects for the estimation of carrier concentrations and effects of complex or line defects are not taken into account. Fig. 3b shows the Fermi level determined through the charge neutrality condition (Eq. (7)) for each oxygen chemical potential. The Fermi level is elevated as the O_2 partial pressure decreases, consistent with experimental observations. The lowest Fermi level (2.34 eV) is reached under O-rich conditions, although it is still much higher than VBM. This indicates that the intrinsic p-type conductivity can never be realized under any equilibrium growth condition. In fact, holes are minority carriers in anatase TiO_2, as shown in Fig. 3(c), in which the carrier densities of electrons and holes defined by Eq. (5) and (6) for each oxygen chemical potential are compared. As expected from Fig. 3c, the electron density increases with decreasing oxygen chemical potential and reaches a very high density (2.32×10^{19} cm^{-3}) for an extremely O-poor condition, which is in a similar order with the experimental result.[15] The result is also consistent with the common observation that electrical conductivity increases with decreasing oxygen partial pressure.[57]

From these results, we conclude that V_{O}^{2+} is the major source of n-type conductivity of anatase TiO_2. This result does not exclude the existence of Ti_i^{4+} because we found that a significant amount of Ti_i^{4+} is present, especially under O-poor conditions (Fig. 3(a)).

Multiple signals electron paramagnetic resonance (EPR) associated with trivalent titanium ions have been observed for reduced anatase TiO_2.[37] The previous theory suggested that the origin of trivalent titanium is either oxygen vacancies or titanium interstitials [11]. Our estimation suggests that the concentration of $[V_{\mathrm{O}}^{1+}]$ is two orders of magnitude higher than that of $[\mathrm{Ti}_i^{3+}]$. Thus, we suggest that the strong EPR signal associated with trivalent titanium originates from $[V_{\mathrm{O}}^{1+}]$.

The single-particle Kohn-Sham levels associated with the neutral and charged defects of

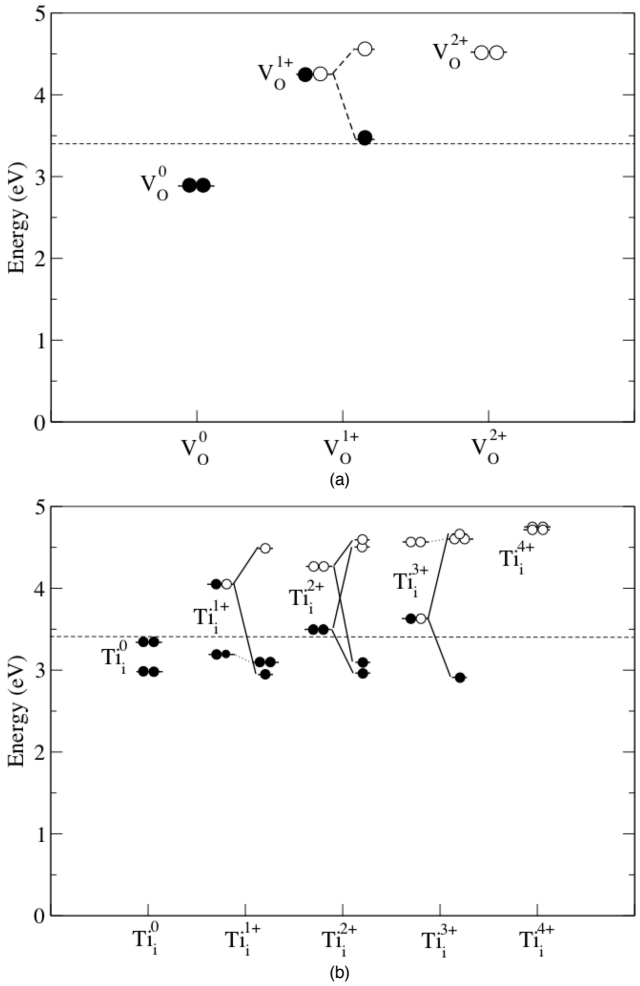

Figure 4: Calculated position of the single-particle state of (a) V_{O} and (b) Ti_i in both non-spin-polarized calculation (left side) and spin-polarized calculation(right side). The calculated adiabatic band gap is represented by dashed lines.

Ti_i and V_{O} are shown in Fig. 4. For charged defects, both spin-up and spin-down channels are depicted along with spin-un-polarized cases. The correction is also necessary for single-particle Kohn-Sham levels according to previous studies.[53, 7, 34] The horizontal dashed line represents an adiabatic computational band gap of 3.73 eV. In Ti_i , the occupied Kohn-Sham levels of the ionized cases are all located lower than those in the neutral case, consistent with the common observation for single ions, i.e., the second-ionization energy is higher than the first-ionization energy. In contrast, the occupied state of V_{O}^{+} lies higher than that of V_{O}^{0}, because of the large atomic relaxations around positively charged

oxygen vacancies. As discussed earlier, the Ti ions that are nearest neighbors to V_{O}^{+} are relaxed outwards, leading to upward shift of the single-particle levels. We found that this effect is more pronounced in our case than in previous studies for rutile TiO_2 using 20% of mixing parameter in HSE.[27]

Thomas *et al.*[54] used X-ray photoelectron spectroscopy (XPS) to find that electron energy loss is 0.9 eV below CBM in rutile and 1.1 eV in anatase. We found that the Kohn-Sham levels of V_{O}^{0} and Ti_i^{3+} are 2.89 and 2.70 eV above the VBM. If we consider the adiabatic computational band gap of 3.73 eV, the defect levels of V_{O}^{0} and Ti_i^{3+} are 0.84 and 1.03 eV below the CBM. The vertical ionization energy measured from XPS is more likely to be originating from Ti_i^{3+}. These species can also be the source of the blue color observed in reduced anatase TiO_2.[48, 49] Note that these occupied charge states are not the predominant form of the defects according to our formation energy analysis (Fig. 2) and their concentrations are therefore limited.

4 Conclusions and Discussion

In summary, due to the failure of the self-interaction error of local and semi-local density functional approximations and their repercussions for polaronic defects, we performed calculations using the Heyd-Scuseria-Ernzerhof (HSE) hybrid functional[21] to gain more insight into the electronic properties of native defects and their likelihood of formation under various growth conditions. The native point defects examined in this study are Ti vacancies (V_{Ti}), O vacancies (V_{O}), Ti interstitials (Ti_i) and O interstitials (O_i). Our calculations showed that V_{O} and Ti_i act as double and quadruple shallow donors, respectively. These defects give rise to high carrier concentration of free electrons from 10^{11} to 10^{19} cm^{-3} in oxygen-rich to oxygen-poor conditions, respectively. On the other hand, V_{Ti} behave as deep acceptors and can alternatively be described as donor compensating defects. We found that hole carriers of these donor-compensating defects are not capable to fully compensate for the free electrons originating from the donor-type defects for any oxygen chemical potential. Under extremely oxygen-rich conditions, the Fermi level is located 2.34 eV above the valence band maximum, indicating that p-type conductivity can never be realized in reality. Our result is consistent with common observations of intrinsic n-type conductivity of TiO_2. At a typical annealing temperature of 550°C and under an oxygen

partial pressure of 10^{-5} Torr, the calculated pinned Fermi level is estimated to be 2.72 eV above the valence band maximum. Note that Fermi-level pinning reported in this work is legitimate only if there is no electrically active impurities. In reality, the absence of active impurities is barely happen in available anatase samples. Under any growth conditions, the concentration of V_{O} was higher than that of Ti_i; therefore, V_{O} is considered the major source of the n-type conductivity in anatase.

Our calculated concentration of V_{O}^{+} is higher than that of Ti_i^{3+}. Consequently, the origin of trivalent titanium ions on reduced TiO_2, observed by EPR measurement, is possibly associated with V_{O}^{+}. In addition, the calculated Kohn-Sham levels associates with V_{O} and Ti_i reveal that vertical ionization measured from XPS originates from Ti_i^{3+}.

5 Output

5.1 International Journal Publication

Adisak Boonchun, Pakpoom Reunchan, and Naoto Umezawa.
"Energetics of native defects in anatase TiO 2: A hybrid density functional study."
Physical Chemistry Chemical Physics 18, 43 (2016): 30040-30046.

5.2 International Conference

The 29th International conference on defects in semiconductor in the topic of "'Energetics of native defects in anatase TiO 2: A hybrid density functional study."
July 31 -Aug 4, 2017, Matsue, Shimane prefecture, Japan

Bibliography

[1] U Bach, D Lupo, P Comte, J E Moser, F Weissörtel, J Salbeck, H Spreitzer, and M Grätzel. Solid-state dye-sensitized mesoporous TiO2 solar cells with high photon-to-electron conversion efficiencies. *Nature*, 395(6702):583–585, 1998.

[2] S A Bilmes, P Mandelbaum, F Alvarez, and N M Victoria. Surface and Electronic Structure of Titanium Dioxide Photocatalysts. *The Journal of Physical Chemistry B*, 104(42):9851–9858, 2000.

[3] P. E. Blöchl. Projector augmented-wave method. *Physical Review B*, 50(24):17953–17979, 1994.

[4] Jeremy K. Burdett, Timothy Hughbanks, Gordon J. Miller, James W. Richardson, and Joseph V. Smith. Structural-electronic relationships in inorganic solids: powder neutron diffraction studies of the rutile and anatase polymorphs of titanium dioxide at 15 and 295 k. *Journal of the American Chemical Society*, 109(12):3639–3646, 1987.

[5] Hungru Chen and James A. Dawson. Molecular oxygen as charge-compensating and magnetic centers in anatase TiO_2. *Phys. Rev. Applied*, 3:064011, Jun 2015.

[6] Xiaobo Chen and Samuel S Mao. Titanium Dioxide Nanomaterials: Synthesis, Properties, Modifications, and Applications. *Chemical Reviews*, 107(7):2891–2959, 2007.

[7] Ismaila Dabo, Boris Kozinsky, Nicholas E Singh-Miller, and Nicola Marzari. Electrostatics in periodic boundary conditions and real-space corrections. *Physical Review B*, 77(11):115139, 2008.

[8] Peter Deák, Bálint Aradi, and Thomas Frauenheim. Polaronic effects in TiO_2 calculated by the HSE06 hybrid functional: Dopant passivation by carrier self-trapping. *Physical ReviewB*, 83(15):155207, April 2011.

[9] Peter Deák, Bálint Aradi, and Thomas Frauenheim. Quantitative theory of the oxygen vacancy and carrier self-trapping in bulk TiO_2. *Physical Review B*, 86:195206, November 2012.

[10] Peter Deák, Bálint Aradi, and Thomas Frauenheim. Oxygen deficiency in TiO_2: Similarities and differences between the ti self-interstitial and the o vacancy in bulk rutile and anatase. *Phys. Rev. B*, 92:045204, Jul 2015.

[11] Cristiana Di Valentin, Gianfranco Pacchioni, and Annabella Selloni. Reduced and n-Type Doped TiO2: Nature of Ti3+ Species. *The Journal of Physical Chemistry C*, 113(48):20543–20552, 2009.

[12] Ulrike Diebold. The surface science of titanium dioxide. *Surface Science Reports*, 48(5):53–229, 2003.

[13] Paul Erhart, Andreas Klein, and Karsten Albe. First-principles study of the structure and stability of oxygen defects in zinc oxide. *Physical Review B*, 72:085213, August 2005.

[14] Emanuele Finazzi, Cristiana Di Valentin, and Gianfranco Pacchioni. Nature of ti interstitials in reduced bulk anatase and rutile tio2. *The Journal of Physical Chemistry C*, 113(9):3382–3385, 2009.

[15] L. Forro, O. Chauvet, D. Emin, L. Zuppiroli, H. Berger, and F. Lévy. High mobility n-type charge carriers in large single crystals of anatase (tio2). *Journal of Applied Physics*, 75(1):633–635, 1994.

[16] A Fujishima and K Honda. Electrochemical Photolysis of Water at a Semiconductor Electrode. *Nature*, 238(5358):37–38, 1972.

[17] Yutaka Furubayashi, Taro Hitosugi, Yukio Yamamoto, Kazuhisa Inaba, Go Kinoda, Yasushi Hirose, Toshihiro Shimada, and Tetsuya Hasegawa. A transparent metal: Nb-doped anatase TiO[sub 2]. *Applied Physics Letters*, 86(25):252101, 2005.

[18] Yutaka Furubayashi, Taro Hitosugi, Yukio Yamamoto, Kazuhisa Inaba, Go Kinoda, Yasushi Hirose, Toshihiro Shimada, and Tetsuya Hasegawa. A transparent metal: Nb-doped anatase tio2. *Applied Physics Letters*, 86(25):252101–252101–3, Jun 2005.

[19] Michael Gratzel. Photoelectrochemical cells. *Nature*, 414(6861):338–344, November 2001.

[20] Marius Grundmann. *The physics of semiconductors: an introduction including devices and nanophysics*. Springer Science & Business Media, 2006.

[21] Jochen Heyd, Gustavo E. Scuseria, and Matthias Ernzerhof. Erratum: "Hybrid functionals based on a screened Coulomb potential" [J. Chem. Phys. [bold 118], 8207 (2003)]. *The Journal of Chemical Physics*, 124(21):219906–219901, 2006.

[22] Yasushi Hirose, Naoomi Yamada, Shoichiro Nakao, Taro Hitosugi, Toshihiro Shimada, and Tetsuya Hasegawa. Large electron mass anisotropy in a d-electron-based transparent conducting oxide: Nb-doped anatase TiO_2 epitaxial films. *Physical Review B*, 79:165108, April 2009.

[23] Taro Hitosugi, Yutaka Furubayashi, Atsuki Ueda, Kinnosuke Itabashi, Kazuhisa Inaba, Yasushi Hirose, Go Kinoda, Yukio Yamamoto, Toshihiro Shimada, and Tetsuya Hasegawa. Ta-doped anatase tio 2 epitaxial film as transparent conducting oxide. *Japanese Journal of Applied Physics*, 44(8L):L1063, 2005.

[24] Taro Hitosugi, Yutaka Furubayashi, Atsuki Ueda, Kinnosuke Itabashi, Kazuhisa Inaba, Yasushi Hirose, Go Kinoda, Yukio Yamamoto, Toshihiro Shimada, and Tetsuya Hasegawa. Ta-doped Anatase TiO_2 Epitaxial Film as Transparent Conducting Oxide. *Japanese Journal of Applied Physics*, 44(34):L1063–L1065, 2005.

[25] Russell F Howe and Michael Gratzel. EPR observation of trapped electrons in colloidal titanium dioxide. *Journal of Physical Chemistry*, 89(21):4495–4499, January 1985.

[26] Hiroshi Irie, Yuka Watanabe, and Kazuhito Hashimoto. Nitrogen-Concentration Dependence on Photocatalytic Activity of TiO2-xNx Powders. *The Journal of Physical Chemistry B*, 107(23):5483–5486, 2003.

[27] A. Janotti, J. B. Varley, P. Rinke, N. Umezawa, G. Kresse, and C. G. Van de Walle. Hybrid functional studies of the oxygen vacancy in TiO_2. *Physical Review B*, 81:085212, February 2010.

[28] Hannu-Pekka Komsa, Tapio T Rantala, and Alfredo Pasquarello. Finite-size supercell correction schemes for charged defect calculations. *Physical Review B*, 86:045112, July 2012.

[29] G. Kresse and J. Furthmüller. Efficiency of ab-initio total energy calculations for metals and semiconductors using a plane-wave basis set. *Computational Materials Science*, 6(1):15–50, 1996.

[30] W. R. L. Lambrecht. Which electronic structure method for the study of defects: A commentary. *Phys Status Solidi B*, 248(7):1547–1558, July 2011.

[31] M Landmann, E Rauls, and W G Schmidt. The electronic structure and optical response of rutile, anatase and brookite TiO_2. *Journal of Physics: Condensed Matter*, 24(19):195503, 2012.

[32] Stephan Lany and Alex Zunger. Assessment of correction methods for the band-gap problem and for finite-size effects in supercell defect calculations: Case studies for ZnO and GaAs. *Physical Review B*, 78:235104, December 2008.

[33] Stephan Lany and Alex Zunger. Polaronic hole localization and multiple hole binding of acceptors in oxide wide-gap semiconductors. *Physical ReviewB*, 80:085202, Aug 2009.

[34] Stephan Lany and Alex Zunger. Many-body gw calculation of the oxygen vacancy in zno. *Physical Review B*, 81(11):113201, 2010.

[35] Bora Lee, Choong-ki Lee, Cheol Seong Hwang, and Seungwu Han. Influence of exchange-correlation functionals on dielectric properties of rutile TiO_2. *Current Applied Physics*, 11(1, Supplement):S293–S296, 2011.

[36] Yu Li, Xiao-Yu Yang, Yi Feng, Zhong-Yong Yuan, and Bao-Lian Su. One-Dimensional Metal Oxide Nanotubes, Nanowires, Nanoribbons, and Nanorods: Syn-

thesis, Characterizations, Properties and Applications. *Critical Reviews in Solid State and Materials Sciences*, 37(1):1–74, 2012.

[37] Stefano Livraghi, Mario Chiesa, Maria Cristina Paganini, and Elio Giamello. On the nature of reduced states in titanium dioxide as monitored by electron paramagnetic resonance. i: The anatase case. *The Journal of Physical Chemistry C*, 115(51): 25413–25421, 2011.

[38] G Makov and M C Payne. Periodic boundary conditions in ab initio calculations. *Physical Review B*, 51:4014–4022, February 1995.

[39] Andrei Malashevich, Manish Jain, and Steven G. Louie. First-principles $DFT + gw$ study of oxygen vacancies in rutile tio_2. *Physical Review B*, 89:075205, Feb 2014.

[40] Yuji Matsumoto, Makoto Murakami, Tomoji Shono, Tetsuya Hasegawa, Tomoteru Fukumura, Masashi Kawasaki, Parhat Ahmet, Toyohiro Chikyow, Shin-ya Koshihara, and Hideomi Koinuma. Room-Temperature Ferromagnetism in Transparent Transition Metal-Doped Titanium Dioxide. *Science*, 291(5505):854–856, 2001.

[41] Benjamin J. Morgan and Graeme W. Watson. Polaronic trapping of electrons and holes by native defects in anatase tio_2. *Physical Review B*, 80:233102, December 2009.

[42] Sutassana Na-Phattalung, M F Smith, Kwiseon Kim, Mao-Hua Du, Su-Huai Wei, S. B. Zhang, and Sukit Limpijumnong. First-principles study of native defects in anatase TiO_2. *Physical Review B*, 73:125205, March 2006.

[43] M K Nowotny, T Bak, and J Nowotny. Electrical Properties and Defect Chemistry of TiO2 Single Crystal. I. Electrical Conductivity†. *The Journal of Physical Chemistry B*, 110(33):16270–16282, 2006.

[44] C. B. Alcock O. Kubaschewski and P. J. Spencer. *Materials Thermochemistry 6th Ed*. Pergamon Press, Oxford, 1993.

[45] Jorge Osorio-Guill 'en, Stephan Lany, and Alex Zunger. Atomic Control of Conductivity Versus Ferromagnetism in Wide-Gap Oxides Via Selective Doping: V, Nb, Ta in Anatase TiO_2. *Physical Review Letters*, 100:036601, January 2008.

[46] John P. Perdew, Kieron Burke, and Matthias Ernzerhof. Generalized Gradient Approximation Made Simple. *Physical Review Letters*, 77:3865–3868, Oct 1996.

[47] Karsten Reuter and Matthias Scheffler. Composition, structure, and stability of RuO_2(110) as a function of oxygen pressure. *Physical Review B*, 65:035406, December 2001.

[48] T Sekiya, K Ichimura, M Igarashi, and S Kurita. Absorption spectra of anatase tio 2 single crystals heat-treated under oxygen atmosphere. *Journal of Physics and Chemistry of Solids*, 61(8):1237–1242, 2000.

[49] Takao Sekiya, Takatoshi Yagisawa, Nozomi Kamiya, Deependra Das Mulmi, Susumu Kurita, Yutaka Murakami, and Tetsuya Kodaira. Defects in anatase tio2 single crystal controlled by heat treatments. *Journal of the Physical Society of Japan*, 73(3):703–710, 2004.

[50] Taishi Sumita, Tetsuya Yamaki, Shunya Yamamoto, and Atsumi Miyashita. Photo-induced surface charge separation of highly oriented TiO_2 anatase and rutile thin films. *Applied Surface Science*, 200(1–4):21–26, 2002.

[51] H. Tang, F. Lévy, H. Berger, and P. E. Schmid. Urbach tail of anatase tio2. *Physical Review B*, 52:7771–7774, Sep 1995.

[52] H. Tang, K. Prasad, R. Sanjinès, P. E. Schmid, and F. Lévy. Electrical and optical properties of tio2 anatase thin films. *Journal of Applied Physics*, 75(4):2042–2047, 1994.

[53] Samuel E Taylor and Fabien Bruneval. Understanding and correcting the spurious interactions in charged supercells. *Physical Review B*, 84(7):075155, 2011.

[54] A G Thomas, W R Flavell, A K Mallick, A R Kumarasinghe, D Tsoutsou, N Khan, C Chatwin, S Rayner, G C Smith, R L Stockbauer, S Warren, T K Johal, S Patel, D Holland, A Taleb, and F Wiame. Comparison of the electronic structure of anatase and rutile TiO_2 single-crystal surfaces using resonant photoemission and x-ray absorption spectroscopy. *Physical Review B*, 75:035105, January 2007.

[55] Naoto Umezawa and Jinhua Ye. Role of complex defects in photocatalytic activities of nitrogen-doped anatase TiO_2. *Physical Chemistry Chemical Physics*, 14:5924–5934, 2012.

[56] T Watanabe, A Nakajima, R Wang, M Minabe, S Koizumi, A Fujishima, and K Hashimoto. Photocatalytic activity and photoinduced hydrophilicity of titanium dioxide coated glass. *Thin Solid Films*, 351(1–2):260–263, 1999.

[57] A. Weibel, R. Bouchet, and P. Knauth. Electrical properties and defect chemistry of anatase (tio2). *Solid State Ionics*, 177(3–4):229 – 236, 2006.

[58] Yu-Xiang Weng, Yong-Qiang Wang, John B Asbury, Hiren N Ghosh, and Tianquan Lian. Back Electron Transfer from TiO2 Nanoparticles to FeIII(CN)63-: Origin of Non-Single-Exponential and Particle Size Independent Dynamics. *The Journal of Physical Chemistry B*, 104(1):93–104, 2000.

[59] Lin-Hui Ye and A. J. Freeman. Defect compensation, clustering, and magnetism in Cr-doped anatase TiO_2. *Physical Review B*, 73:081304, February 2006.

6 Appendix

PCCP

Accepted Manuscript

This article can be cited before page numbers have been issued, to do this please use: A. Boonchun, P. Reunchan and N. Umezawa, *Phys. Chem. Chem. Phys.*, 2016, DOI: 10.1039/C6CP05798E.

ROYAL SOCIETY OF CHEMISTRY

www.rsc.org/pccp

View Article Online
DOI: 10.1039/C6CP07985E
ARTICLE TYPE www.rsc.org/xxxxxx | XXXXXXXX

Energetics of native defects in anatase TiO_2: A hybrid density functional study†

Adisak Boonchun,[a,b] Pakpoom Reunchan,[a] and Naoto Umezawa[b,c,*]

Received Xth XXXXXXXXXX 20XX, Accepted Xth XXXXXXXXX 20XX
First published on the web Xth XXXXXXXXXX 200X
DOI: 10.1039/b000000x

The energetics and electronic structures of native defects in anatase TiO_2 are comprehensively studied using hybrid density functional calculations. We demonstrate that oxygen vacancies (V_O) and titanium interstitials (Ti_i) act as shallow donors, and can form with substantial concentrations, giving rise to free electrons with carrier densities from 10^{11} to 10^{19} cm^{-3} for oxygen-rich and oxygen-poor conditions, respectively. The titanium vacancies (V_{Ti}), identified as deep acceptors and induced hole carriers, are incapable of fully compensating for the free electrons originating from the donor-type defects at any oxygen chemical potential. Even under an extreme oxygen-rich condition, the Fermi level, which is determined from the charge neutrality condition among charge defects, electron and hole carriers are located 2.34 eV above the valence band maximum, indicating that *p*-type conductivity can never be realized under any growth conditions without external doping. This is consistent with common observations of intrinsic *n*-type conductivity of TiO_2. At a typical annealing temperature and under a typical oxygen partial pressure, the carrier concentration is found to be approximately 5×10^{13} cm^{-3}.

1 Introduction

TiO_2 is a technologically important wide-bandgap semiconductor with applications as a transparent conducting oxide (TCO),[1,2] in photocatalysis,[3] solar cells[4,5] and as a ferromagnetic wide-bandgap oxide.[6,7] TiO_2 exists as three polymorphs: rutile, anatase, and brookite. Anatase has been a favored phase for nanopowdered photocatalytic applications due to its higher activity than rutile[8,9], although nanostructures like nanorods and nanotubes with rutile structure have also been synthesized.[10,11] Anatase phase is important for TCO applications possibly due to its smaller electron-effective mass than rutile. There are several reports on doping for *n*-type conductivity of anatase TiO_2-based TCO,[1,12–15] reports on *p*-type conductivity are very rare. The photoexcitation of electron-hole pairs in pristine TiO_2 requires relatively high photon energy and occurs only under ultraviolet light. In practice, reduced TiO_2 can absorb photon in visible light region according to the abundance of trivalent Ti (Ti^{3+}).[16,17] Reduced TiO_2 also exhibits *n*-type conductivity,[18–20] the origin of which was proposed to be donor-type defects like oxygen vacancies (V_O) and titanium interstitials (Ti_i).[18] First-principles calculations based on density functional theory (DFT) have been established as an important tool for understanding and acquiring knowledge of native defects in general.

Native defects in anatase TiO_2 were previously studied using local-density approximation (LDA) and generalized gradient approximation (GGA).[21,22] However, recent studies revealed that self-interaction correction and its repercussions for polaronic effects are important for discussing electronic and magnetic properties of native defects in metal oxides.[23] The approximation methods that include some of the essential correlation- or orbital-dependent effects, such as LDA+*U* (or GGA+*U*) and hybrid functionals, are more insightful for understanding of and gaining knowledge about native defects. Morgan and Watson[24] reported a GGA+*U* study of the transition levels and single-particle levels of donor- and acceptor-type native defects in anatase TiO_2. They suggested that V_O and Ti_i are deep donors that donate two and four electrons, respectively, whereas V_{Ti} are deep acceptors generating four holes.

Since Heyd-Scuseria-Ernzerhof (HSE) hybrid functional[25] yields a better description of bandgap, it should also be useful for accurate estimations of the defect levels in semiconductors and metal oxides. Janotti *et al.*[26] performed HSE hybrid functional calculations on rutile TiO_2 and showed that oxygen vacancies are stable in their positively charged states V_O^{2+} for any Fermi energy within the bandgap, indicating that they are shallow donors. Recently, P. Deák *et al.*[27] also stud-

† Electronic Supplementary Information (ESI) available: The optimized structure of native defect in anatase TiO2 and . See DOI: 10.1039/b000000x/

[a] *Department of Physics, Faculty of Science, Kasetsart University, Bangkok 10900, Thailand.*
[b] *International Center for Materials Nanoarchitectonics (MANA), National Institute for Materials Science, 1-1 Namiki, Tsukuba, Ibaraki 305-0044, Japan*
[c] *Center for Materials research by Information Integration (CMI^2), National Institute for Materials Science, 1-2-1 Sengen, Tsukuba, Ibaraki 305-0047, Japan*
[*] *Corresponding author; E-mail:UMEZAWA.Naoto@nims.go.jp;*

View Article Online
DOI: 10.1039/C6CP05798E

ied oxygen vacancies and carrier self-trapping in anatase and rutile TiO_2 using HSE06,[25] and showed that oxygen vacancies are shallow donors in both anatase and rutile phases. Finazzi *et al.*[28] demonstrated using GGA+U (with U=4 eV) or B3LYP hybrid functional that charge-neutral oxygen vacancies in anatase TiO_2 create defect states at 1 eV below the conduction band. Recently, P. Deák *et al.*[29] found that oxygen vacancies and titanium interstitial are both shallow donors by using HSE06. The single-particle Kohn-Sham levels associated with Ti interstitials were also investigated using spin-polarized hybrid DFT.[28] Malashevich *et al.*[30] studied oxygen vacancies in rutile structure using DFT+GW, and found that the transition level of charged states from +2 to +1, $\varepsilon(+2/+1)$, is higher than that of +2 to neutral, $\varepsilon(+2/0)$, showing negative U behavior. From their estimation $\varepsilon(+2/0)$ lies 2.8 eV above the VBM.

These theoretical studies mainly focused on the identification of defect levels and the validation of computational results obtained from the different methods. However the Fermi level position and carrier concentrations in intrinsic anatase TiO_2 have not been quantitatively estimated. Moreover, the origin of the n-type conductivity is still controversial and a theoretical study based on accurate computational methods is required. In this study, we employ the HSE06 hybrid functional, which was proven to be reliable for defect calculations in TiO_2,[31] to conduct a comprehensive study for the energetics of native defects in anatase TiO_2 and to estimate carrier concentration under a given oxygen partial pressure. Since the antisite defects (Ti_O and O_{Ti}) have high formation energies,[21] they are not considered in the present study. The native point defects examined in this study are V_{Ti}, V_O, Ti_i and O interstitials (O_i) in anatase TiO_2.

2 Computational method

Our study is based on DFT calculations using the HSE hybrid functional.[25] The calculations were performed using the VASP code[32] with the projector-augmented wave (PAW) method.[33] We used a well-converged energy cut-off of 400 eV for the projector-augmented plane waves. In conventional unit cells, the Brillouin zone is expressed using $5 \times 5 \times 5$ Monkhorst-Pack meshes.

For Ti, $3s^2 3p^6 4s^2 3d^2$ states were treated as valence states. In the HSE approach, the Coulomb potential in the exchange energy is divided into short-range and long-range parts with a screening length of 10 Å. In the short-range part, the non-local Hartree-Fock (HF) exchange is mixed with the Perdew, Burke, and Ernzerhof (PBE) GGA exchange energy.[34] The long-range part and the correlation potential are represented by the PBE functional.

We used the standard HF mixing $\alpha = 0.25$ which is suitable for satisfaction of the generalized Koopmans' theorem[35] in both anatase and rutile TiO_2[31]. The geometry relaxation was performed for a cell volume and shape, as well as for atomic positions of 12-atom conventional cell, until the residual force is less than 0.02 eV/Å. Our calculated lattice constants are a=3.760 Å and c=9.621 Å, which were close to other HSE06-reported constants of a=3.755 Å and c=9.561 Å,[31] and experimental results: a=3.782 Å and c=9.502 Å.[36]

Our calculated indirect bandgap is 3.73 eV for the transition from the valence band maximum (VBM) near M point (0.425, 0.425, 0) to the conduction band minimum (CBM) at Γ. Although we attempted to use the same cut-off energy and valence electron configuration potentials as were used in previous HSE06 calculation,[31] we somehow still obtained a larger bandgap, which is accidentally equal to the adiabatic bandgap of G_0W_0 calculation (3.73 eV).[37] Note that, both HSE06 and quasi-particle G_0W_0 bandgaps are higher than the experimentally measured optical bandgap (3.42 eV)[38]

For defect calculation, we extended the conventional cell by $3\times3\times1$ to produce a 108-atom supercell and introduced a defect in the supercell. K-points were sampled at a Monkhorst-Pack special $1 \times 1 \times 1$ mesh for the Brillouin zone integration of the supercell. Calculations for charged states were also performed for each defect with neutralizing background charge. The charged states considered here are (+2, +1, 0) for V_O, (+4, +3, +2, +1, 0) for Ti_i, (-4, -3, -2, -1, 0) for V_{Ti} and (+2, +1, 0) for O_i. The effects of spin polarization were included for all charged states. Relaxations were performed for atomic positions with a fixed cell volume until the residual force is less than 0.02 eV/Å.

Fictitious interactions between the charged defect with its images in neighboring cells and with the homogeneous background charge were removed using the scheme proposed by Makov and Payne.[39] Normally, the quadrupole term in the Makov and Payne correction can be approximated to about one-third of the monopole term for cubic supercells as reported by Lany and Zunger.[40] Since the supercell used in this study is non-cubic, the non-cubic adjustment[41] has been used to correct the quadrupole term in Makov and Payne. The dielectric constant is needed in the Makov and Payne correction. From HSE calculations for dielectric constants of anatase TiO_2,[42] the average value of 46.23 was used in the correction.

To ensure the convergence of the cell size, especially for high-charge-state defects, we tested the formation energy calculations of oxygen vacancies in neutral charged states with a larger supercell size of 216 atoms, i.e. $3 \times 3 \times 2$ extension of the conventional cell. We found that the formation energy of neutral charge V_O is changed only by 0.075 eV as cell size increased from 108 to 216 atoms. The relaxed geometries for all defects examined are shown in [Electronic Supporting Information]

To identify the dominant type of native defect, we compared the stabilities of Ti_i, V_{Ti}, V_O and O_i. The formation energy of

View Article Online
DOI: 10.1039/C6CP05798E

a native defect D with charge state q is defined as

$$E_f(D^q) = E_{tot}(D^q) - E_{tot}(\mathrm{TiO_2}) - \mathrm{n_i}\mu_\mathrm{i} + q(\varepsilon_\mathrm{F} + E_\mathrm{V}), \quad (1)$$

where $E_{tot}(D^q)$ is the total energy of the cell with defect D in charge state q. $E_{tot}(\mathrm{TiO_2})$ is the total energy of the cell without defects, $\mathrm{n_i}$ is the number of atoms of species i (Ti or O) that have been added to ($\mathrm{n_i} > 0$) or removed from ($\mathrm{n_i} < 0$) the supercell. ε_F is the Fermi energy that ranged over the bandgap. Note that ε_F is the energy of the electron reservoir with respect to the VBM, E_V, which is corrected in a defect-containing supercell by aligning the electrostatic potential at a region far away from the defect site with the corresponding potential in a perfect crystal.

Finally, μ_i is a chemical potential representing the energy for defect D that is taken from reservoir. We reference chemical potentials $\tilde{\mu}_i$ to the energy per atom of isolated elemental phase: $\tilde{\mu}_\mathrm{O} = \mu_\mathrm{O} - \frac{1}{2}E_{tot}[\mathrm{O_2}]$ and $\tilde{\mu}_\mathrm{Ti} = \mu_\mathrm{Ti} - E_{tot}[\mathrm{Ti}_{bulk}]$. These reference energies are given by our DFT calculations for a total energy of bulk Ti per formula unit (-9.46 eV) and a half of total energy of an isolated O_2 molecule (-8.55 eV).

The chemical potential is a variable but it must satisfy the thermodynamic equilibrium condition of TiO_2, $\tilde{\mu}_\mathrm{Ti} + 2\tilde{\mu}_\mathrm{O} = \Delta H_f(\mathrm{TiO_2})$ where $\Delta H_f(\mathrm{TiO_2})$ is the formation enthalpy of TiO_2. At the oxygen-rich limit ($\tilde{\mu}_\mathrm{O}$=0), the chemical potential of Ti is given by $\tilde{\mu}_\mathrm{Ti} = \Delta H_f(\mathrm{TiO_2})$. At the Ti-rich limit, $\tilde{\mu}_\mathrm{Ti}$ is bounded by the formation of Ti_2O_3, $2\tilde{\mu}_\mathrm{Ti} + 3\tilde{\mu}_\mathrm{O} < \Delta H_f(\mathrm{Ti_2O_3})$.[21] The formation enthalpies estimated using the HSE approach are $\Delta H_f(\mathrm{TiO_2})$= -9.756 eV and $\Delta H_f(\mathrm{Ti_2O_3})$= -15.493 eV which are in good agreement with the previous report.[43,44] After all, the chemical potential settings ($\tilde{\mu}_\mathrm{Ti}$, $\tilde{\mu}_\mathrm{O}$) corresponding to Ti-rich (O-poor) and O-rich (Ti-poor) are (-1.72,-4.02) and (-9.76, 0) in eV, respectively.

In addition to the extreme chemical potential conditions (Ti-rich and O-rich), we consider an intermediate oxygen chemical potential corresponding to a realistic growth condition during the annealing of anatase TiO_2. The oxygen chemical potential is a function of temperature and oxygen partial pressure, as described by[45]

$$\tilde{\mu}_\mathrm{O}(T,p) = \tilde{\mu}_\mathrm{O}(T,p_0) + \frac{1}{2}k_B T \ln(p/p_0), \quad (2)$$

where $\tilde{\mu}_\mathrm{O}(T,p_0)$ is the oxygen chemical potential at the standard pressure $p_0 = 1$ atm, k_B is Bolzmann's constant, and T is the temperature in Kelvin. The typical annealing temperature used in the growth of anatase TiO_2 is 400-550°C[1,2,46] and the typical oxygen partial pressure is 10^{-4}-10^{-5} Torr.[47] We therefore choose an annealing temperature of 550°C and an oxygen partial pressure of 10^{-5} Torr, which corresponds to ($\tilde{\mu}_\mathrm{Ti}$, $\tilde{\mu}_\mathrm{O}$) = (-6.70, -1.52) in eV.

The thermodynamic transition levels are given by the Fermi energy at which the formation energies of the two charged states are equal [Supporting information]:

$$\varepsilon_D(q/q') = \frac{E_f(D^q;\varepsilon_F=0) - E_f(D^{q'};\varepsilon_F=0)}{q'-q} \quad (3)$$

which thermodynamic transition represented by kinks in the plots of formation energy as a function of Fermi energy. Note that ε_F ranges over the bandgap and references to the VBM.

The concentration of a native defect D with charge q, c(D^q), is related to its formation energy E_f through the equation

$$c(D^q) = N_\mathrm{sites}/(1+\exp^{E_f(D^q)/k_BT}), \quad (4)$$

where N_sites is the number of possible lattice sites per unit volume (V_cell) at which the defect can be formed.

The hole concentration (p) and electron concentration (n) can be expressed by the following equations:[48]

$$n = 2\left(\frac{m_e k_B T}{2\pi\hbar^2}\right)^{3/2} \exp^{(\varepsilon_F - \mathrm{E_g})/k_B T}, \quad (5)$$

$$p = 2\left(\frac{m_h k_B T}{2\pi\hbar^2}\right)^{3/2} \exp^{-\varepsilon_F/k_B T}, \quad (6)$$

where m_e, m_h are the electron- and hole-effective masses, respectively, and E_g is the bandgap. The charge neutrality is satisfied when the summation of donor and electron carrier concentrations equals the acceptor and hole carrier concentrations,

$$\sum_i q_i c_i(D^q) + p - n = 0. \quad (7)$$

The index i represents donor- or acceptor-type defect. In our calculations, the experimental hole-effective mass of $0.8m_0$ and electron effective mass of $1.2m_0$ were used.[49]

3 Results

Figure. 1 shows the formation energies obtained from our hybrid DFT calculations as a function of the Fermi energy. The lower and upper limits of the Fermi energy correspond to the VBM and CBM, respectively. The slope of each line reflects the stable charged state of each defect, *e.g.* V_O^{2+} is stable over the other charged states of V_O in the entire range of Fermi energies. The transition levels $\varepsilon(q/q')$ corresponding to each defect are listed in Table. 1, some of which are also shown as filled circles in Fig. 1

Under Ti-rich conditions (Fig. 1(a)), Ti_i^{4+} has the lowest formation energy among the defects examined over a wide range of Fermi energies. However, the predominance overturns at a higher Fermi energy, i.e. the formation energy of V_O^{2+} is slightly lower than that of Ti_i^{4+} near CBM. On the

View Article Online
DOI: 10.1039/C6CP05798E

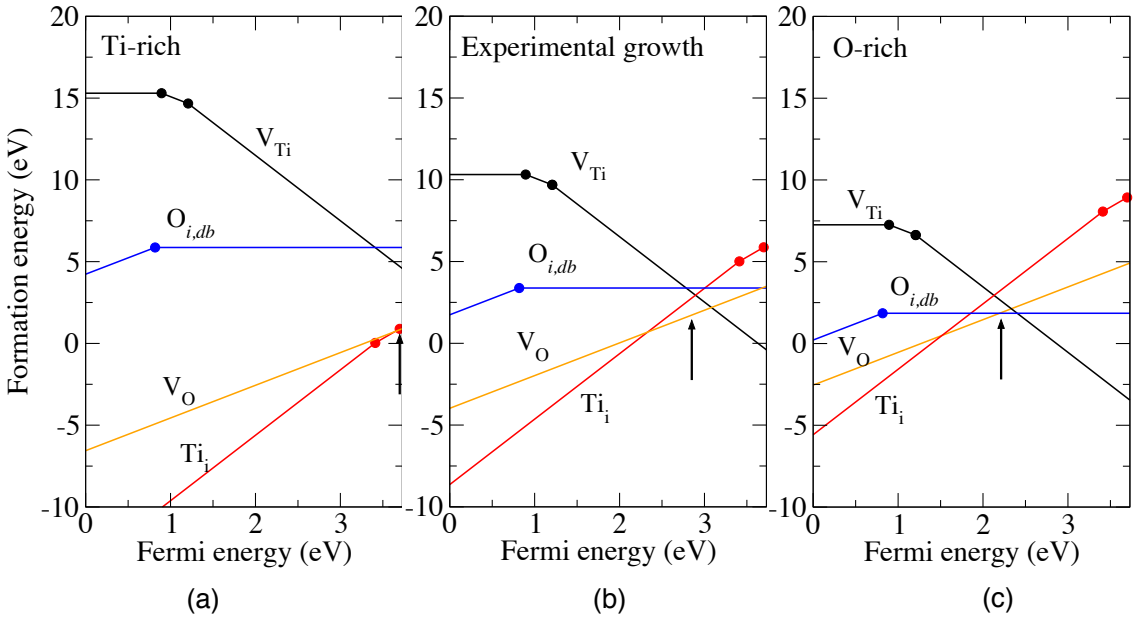

Fig. 1 Defect formation energies as a function of Fermi energy under (a) Ti-rich, (b) experimental growth, and (c) O-rich conditions. The up-pointing arrow indicates the Fermi level determined by the charge neutrality condition at 550 °C.

Table 1 The transition level $\varepsilon(q,q')$ all in eV reference to the VBM

Defect	q,q'	$\varepsilon(q,q')$
V_O	+2/+	3.92
	+2/0	3.82
Ti_i	+4/+3	3.41
	+3/+2	3.70
	+2/+1	3.82
	+1/0	4.01
V_{Ti}	0/-2	0.89
	-2/-4	1.21
O_i	+2/0	0.81

other hand, the formation energy of V_{Ti}^{4-} is higher than those of V_O^{2+} and Ti_i^{4+} at any Fermi level, indicating that hole carriers induced by the acceptor-type defect (V_{Ti}^{4-}) are incapable of compensating for electrons induced by the donor-type defects (V_O^{2+} and Ti_i^{4+}). In fact, the Fermi level determined by the charge neutrality condition under a typical annealing temperature of 550 °C is pinned at the CBM under the Ti-rich condition according to our following analysis. The pinned Fermi levels are denoted as up-pointing arrows in Fig. 1 for each $\tilde{\mu}_O$ condition. When the transition level is above CBM, Fermi level is considered pinned at the CBM. At the oxygen-rich limit, the formation energy of V_{Ti}^{4-} is lowered and the carrier compensation effect is more pronounced, as observed in the downward shift of the Fermi level, although it is still higher than the VBM by 2.34 eV and cannot reach p-type conductivity (Fig. 1(c)). Here, the formation of V_O^{2+} is still favored compared to Ti_i^{4+} at the pinned Fermi level. Under an intermediate μ_O corresponding to an experimental growth condition (oxygen partial pressure 10^{-5} Torr at 550 °C)[47], the Fermi level is located at 2.72 eV. Again, V_O^{2+} predominates over Ti_i^{4+} at the pinned Fermi level (Fig. 1(b)), and therefore is considered the major source of electron carriers. Thus, V_O^{2+} is the predominant donor-type defect under any $\tilde{\mu}_O$ condition.

Ti_i is stable in the form of quadruple charged state. The nearest oxygen neighbor along the vertical c-axis relaxes inward by 23.6% in Ti_i while the two nearest-neighbor oxygen atoms on the basal axis relax outward by only 0.37%. The optimized structure of Ti_i is shown in ESI Fig. S1.(b). Most of the thermodynamic transition levels for Ti_i shown in Table I are located above the CBM, reflecting that it is a shallow donor.

V_O is stable in the doubly charged state. There are three nearest-neighbors Ti atoms around V_O. In neutral charge state, one Ti nearest-neighbor relaxes outwards by 8.39% while the other two relax outwards by 2.80%. The optimized structure of V_O is shown in ESI Fig. S1.(c). The transition levels $\varepsilon(+2/+)$ and $\varepsilon(+2/0)$ (not shown in Fig. 1) are located above the CBM, which is consistent with previous reports using the HSE approach for rutile[26] and antase[29]. Note that in our HSE06 calculation, we used low-frequency limit of the

View Article Online
DOI: 10.1039/C6CP05798E

dielectric constant in Lany-Zunger charge correction[40] while P. Deák *et al.*[29] applied high-frequency dielectric constant in Lany-Zunger charge correction. Interestingly, our calculation and P. Deák *et al.*[29] yield qualitatively consistent results in terms of the point that both V_O and Ti_i exhibit the nature of shallow donors. By contrast, DFT+U predicted they are deep donors.[24,43]

O_i atoms are more stable in dumbbell configuration ($O_{i,db}$) than in an octahedral configuration ($O_{i,oct}$), in the form of peroxide ions at oxygen lattice sites. All the neighboring Ti atoms relax outward only slightly. The optimized structure of $O_{i,db}$ is shown in ESI Fig. S1.(d). Substitutional O_2 has a bond length of 1.44 Å in the neutral charge state, which is slightly longer than that in an isolated O_2 molecule (1.21 Å). The transition level $\varepsilon(+2/0)$ is located 0.81 eV above the VBM, indicating that it is a deep donor. The detailed analysis of O_i have been studied by Paul Erhart *et al.*[50]

V_{Ti} defect changes its charge state from neutral to -2 to -4 as the Fermi energy increases, as shown in Fig. 1. The thermodynamic transition levels are located in the band gap: $\varepsilon(0/-2)$ = 0.89 and $\varepsilon(-2/-4)$ = 1.21 eV, which indicates that V_{Ti} is a deep acceptor. Recently, Chen and Dawson show that V_{Ti} is not stable with respect to the complex defect $V_{Ti} + 2V_O + O_2$ for the Fermi level less than 1.37 eV by using HSE06.[51] The formation energy of this complex is very high and does not contribute in our charge neutrality calculation. In anatase, the axial bond lengths are longer than the equatorial bond lengths. The nearest-neighbor oxygen atoms in the basal plane containing V_{Ti}^{4-} relax outwards by 4.6%, whereas the nearest-neighbor oxygen atoms in the axial direction relax outwards by 20%. The optimized structure of V_{Ti} is shown in ESI Fig. S1.(e).

Fig. 2(a) shows defect concentrations as a function of oxygen chemical potential or oxygen partial pressure at 550°C. Note that Eq. 7 is satisfied for each oxygen chemical potential in the plots shown in Fig.2. It is clear that the concentration of V_O^{2+} is higher than that of Ti_i^{4+} for any oxygen chemical potential, while the concentration of V_{Ti}^{4-} is limited. Note that we considered only point defects for the estimation of carrier concentrations and effects of complex or line defects are not taken into account. Fig. 2b shows the Fermi level determined through the charge neutrality condition (Eq. (7)) for each oxygen chemical potential. The Fermi level is elevated as the O_2 partial pressure decreases, consistent with experimental observations. The lowest Fermi level (2.34 eV) is reached under O-rich conditions, although it is still much higher than VBM. This indicates that the intrinsic p-type conductivity can never be realized under any equilibrium growth condition. In fact, holes are minority carriers in anatase TiO_2, as shown in Fig. 2(c), in which the carrier densities of electrons and holes defined by Eq. (5) and (6) for each oxygen chemical potential are compared. As expected from Fig. 2c, the electron density increases with decreasing oxygen chemical potential and reaches a very high density (2.32×10^{19} cm^{-3}) for an extremely O-poor condition, which is in a similar order with the experimental result.[13] The result is also consistent with the common observation that electrical conductivity increases with decreasing oxygen partial pressure.[52]

From these results, we conclude that V_O^{2+} is the major source of n-type conductivity of anatase TiO_2. This result does not exclude the existence of Ti_i^{4+} because we found that a significant amount of Ti_i^{4+} is present, especially under O-poor conditions (Fig. 2(a)).

Multiple signals electron paramagnetic resonance (EPR) associated with trivalent titanium ions have been observed for reduced anatase TiO_2.[53] The previous theory suggested that the origin of trivalent titanium is either oxygen vacancies or titanium interstitials[17]. Our estimation suggests that the concentration of $[V_O^{1+}]$ is two orders of magnitude higher than that of $[Ti_i^{3+}]$. Thus, we suggest that the strong EPR signal associated with trivalent titanium originates from $[V_O^{1+}]$.

The single-particle Kohn-Sham levels associated with the neutral and charged defects of Ti_i and V_O are shown in Fig. 3. For charged defects, both spin-up and spin-down channels are depicted along with spin-un-polarized cases. The correction is also necessary for single-particle Kohn-Sham levels according to previous studies.[54–56] The horizontal dashed line represents an adiabatic computational band gap of 3.73 eV. In Ti_i , the occupied Kohn-Sham levels of the ionized cases are all located lower than those in the neutral case, consistent with the common observation for single ions, i.e., the second-ionization energy is higher than the first-ionization energy. In contrast, the occupied state of V_O^+ lies higher than that of V_O^0, because of the large atomic relaxations around positively charged oxygen vacancies. As discussed earlier, the Ti ions that are nearest neighbors to V_O^+ are relaxed outwards, leading to upward shift of the single-particle levels. We found that this effect is more pronounced in our case than in previous studies for rutile TiO_2 using 20% of mixing parameter in HSE.[26]

Thomas *et al.*[57] used X-ray photoelectron spectroscopy (XPS) to find that electron energy loss is 0.9 eV below CBM in rutile and 1.1 eV in anatase. We found that the Kohn-Sham levels of V_O^0 and Ti_i^{3+} are 2.89 and 2.70 eV above the VBM. If we consider the adiabatic computational band gap of 3.73 eV, the defect levels of V_O^0 and Ti_i^{3+} are 0.84 and 1.03 eV below the CBM. The vertical ionization energy measured from XPS is more likely to be originating from Ti_i^{3+}. These species can also be the source of the blue color observed in reduced anatase TiO_2.[58,59] Note that these occupied charge states are not the predominant form of the defects according to our formation energy analysis (Fig. 1) and their concentrations are therefore limited.

View Article Online
DOI: 10.1039/C6CP05798E

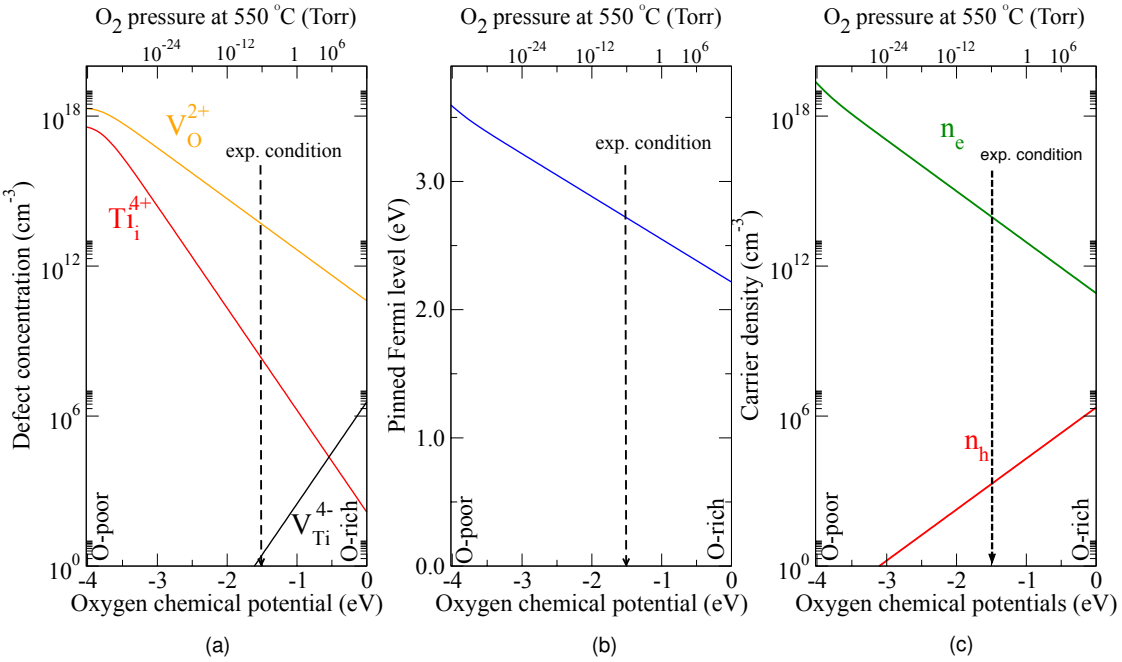

Fig. 2 (a) The defect concentration (b) pinned Fermi energy and (c) carrier concentration (electrons n_e and holes n_h) as a function of oxygen chemical potentials. The down-pointing arrow with the vertical dashed line indicates the oxygen chemical potential, -1.52 eV, corresponding to the experimental condition at the annealing temperature of 550°C and under an oxygen partial pressure of 10^{-5} Torr.

4 Conclusions

In summary, due to the failure of the self-interaction error of local and semi-local density functional approximations and their repercussions for polaronic defects, we performed calculations using the Heyd-Scuseria-Ernzerhof (HSE) hybrid functional[25] to gain more insight into the electronic properties of native defects and their likelihood of formation under various growth conditions. The native point defects examined in this study are Ti vacancies (V_{Ti}), O vacancies (V_{O}), Ti interstitials (Ti_i) and O interstitials (O_i). Our calculations showed that V_{O} and Ti_i act as double and quadruple shallow donors, respectively. These defects give rise to high carrier concentration of free electrons from 10^{11} to 10^{19} cm^{-3} in oxygen-rich to oxygen-poor conditions, respectively. On the other hand, V_{Ti} behave as deep acceptors and can alternatively be described as donor compensating defects. We found that hole carriers of these donor-compensating defects are not capable to fully compensate for the free electrons originating from the donor-type defects for any oxygen chemical potential. Under extremely oxygen-rich conditions, the Fermi level is located 2.34 eV above the valence band maximum, indicating that *p*-type conductivity can never be realized in reality. Our result is consistent with common observations of intrinsic *n*-type conductivity of TiO_2. At a typical annealing temperature of 550°C and under an oxygen partial pressure of 10^{-5} Torr, the calculated pinned Fermi level is estimated to be 2.72 eV above the valence band maximum. Note that Fermi-level pinning reported in this work is legitimate only if there is no electrically active impurities. In reality, the absence of active impurities is barely happen in available anatase samples. Under any growth conditions, the concentration of V_{O} was higher than that of Ti_i; therefore, V_{O} is considered the major source of the n-type conductivity in anatase.

Our calculated concentration of V_{O}^{+} is higher than that of Ti_i^{3+}. Consequently, the origin of trivalent titanium ions on reduced TiO_2, observed by EPR measurement, is possibly associated with V_{O}^{+}. In addition, the calculated Kohn-Sham levels associates with V_{O} and Ti_i reveal that vertical ionization measured from XPS originates from Ti_i^{3+}.

5 Acknowledgments

N. U. was partly supported by the Japan Science and Technology Agency (JST) Precursory Research for Embryonic Science and Technology (PRESTO) and the Core Research for Evolutional Science and Technology (CREST) programs. A. B. was supported by Thailand Research Fund for New Researcher (TRG5780264) and Kasetsart University Research

View Article Online
DOI: 10.1039/C6CP05798E

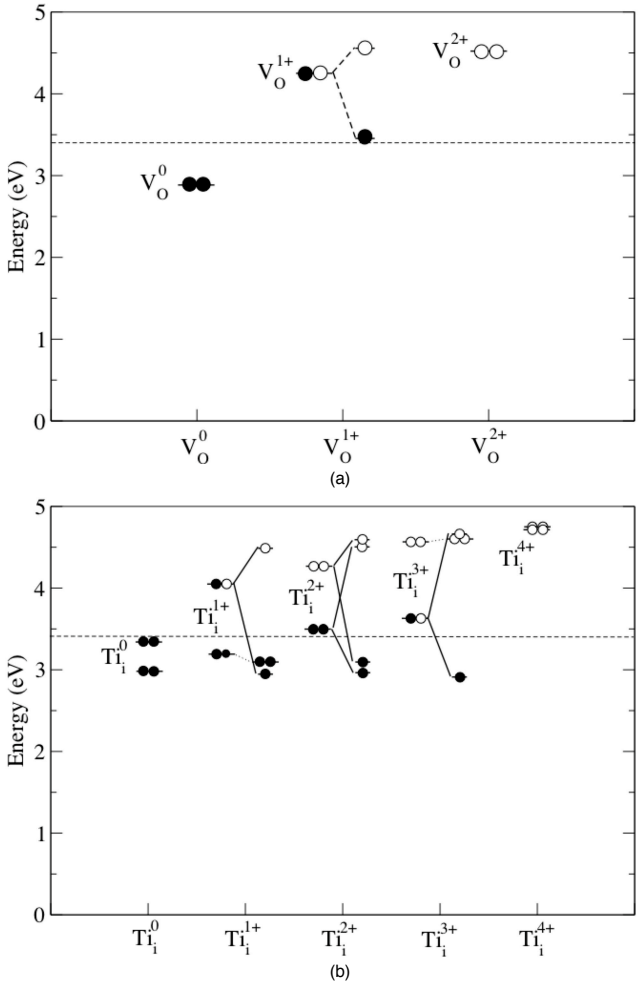

Fig. 3 Calculated position of the single-particle state of (a) V_O and (b) Ti_i in both non-spin-polarized calculation (left side) and spin-polarized calculation(right side). The calculated adiabatic band gap is represented by dashed lines.

and Development Institute (KURDI). P. R. was supported by KURDI. We wish to thank High-performance computing facilities King Mongkut's University of Technology Thonburi (KMUTT, Thailand) for their hospitality. We acknowledge A. Janotti, S. Limpijumnong and J. B. Varley for fruitful discussions. We also thank J. Ye and H. Abe for their support.

References

1 Y. Furubayashi, T. Hitosugi, Y. Yamamoto, K. Inaba, G. Kinoda, Y. Hirose, T. Shimada and T. Hasegawa, *Applied Physics Letters*, 2005, **86**, 252101.

2 T. Hitosugi, Y. Furubayashi, A. Ueda, K. Itabashi, K. Inaba, Y. Hirose, G. Kinoda, Y. Yamamoto, T. Shimada and T. Hasegawa, *Japanese Journal of Applied Physics*, 2005, **44**, L1063–L1065.

3 A. Fujishima and K. Honda, *Nature*, 1972, **238**, 37–38.

4 M. Gratzel, *Nature*, 2001, **414**, 338–344.

5 U. Bach, D. Lupo, P. Comte, J. E. Moser, F. Weissörtel, J. Salbeck, H. Spreitzer and M. Grätzel, *Nature*, 1998, **395**, 583–585.

6 Y. Matsumoto, M. Murakami, T. Shono, T. Hasegawa, T. Fukumura, M. Kawasaki, P. Ahmet, T. Chikyow, S.-y. Koshihara and H. Koinuma, *Science*, 2001, **291**, 854–856.

7 L.-H. Ye and A. J. Freeman, *Physical Review B*, 2006, **73**, 081304.

8 T. Sumita, T. Yamaki, S. Yamamoto and A. Miyashita, *Applied Surface Science*, 2002, **200**, 21–26.

9 T. Watanabe, A. Nakajima, R. Wang, M. Minabe, S. Koizumi, A. Fujishima and K. Hashimoto, *Thin Solid Films*, 1999, **351**, 260–263.

10 Y. Li, X.-Y. Yang, Y. Feng, Z.-Y. Yuan and B.-L. Su, *Critical Reviews in Solid State and Materials Sciences*, 2012, **37**, 1–74.

11 X. Chen and S. S. Mao, *Chemical Reviews*, 2007, **107**, 2891–2959.

12 H. Tang, K. Prasad, R. Sanjins, P. E. Schmid and F. Lvy, *Journal of Applied Physics*, 1994, **75**, 2042–2047.

13 L. Forro, O. Chauvet, D. Emin, L. Zuppiroli, H. Berger and F. Lvy, *Journal of Applied Physics*, 1994, **75**, 633–635.

14 Y. Furubayashi, T. Hitosugi, Y. Yamamoto, K. Inaba, G. Kinoda, Y. Hirose, T. Shimada and T. Hasegawa, *Applied Physics Letters*, 2005, **86**, 252101–252101–3.

15 T. Hitosugi, Y. Furubayashi, A. Ueda, K. Itabashi, K. Inaba, Y. Hirose, G. Kinoda, Y. Yamamoto, T. Shimada and T. Hasegawa, *Japanese Journal of Applied Physics*, 2005, **44**, L1063.

16 R. F. Howe and M. Gratzel, *Journal of Physical Chemistry*, 1985, **89**, 4495–4499.

17 C. Di Valentin, G. Pacchioni and A. Selloni, *The Journal of Physical Chemistry C*, 2009, **113**, 20543–20552.

18 U. Diebold, *Surface Science Reports*, 2003, **48**, 53–229.

19 S. A. Bilmes, P. Mandelbaum, F. Alvarez and N. M. Victoria, *The Journal of Physical Chemistry B*, 2000, **104**, 9851–9858.

20 M. K. Nowotny, T. Bak and J. Nowotny, *The Journal of Physical Chemistry B*, 2006, **110**, 16270–16282.

21 S. Na-Phattalung, M. F. Smith, K. Kim, M.-H. Du, S.-H. Wei, S. B. Zhang and S. Limpijumnong, *Physical Review B*, 2006, **73**, 125205.

22 J. Osorio-Guill 'en, S. Lany and A. Zunger, *Physical Review Letters*, 2008, **100**, 036601.

23 W. R. L. Lambrecht, *Phys Status Solidi B*, 2011, **248**, 1547–1558.

24 B. J. Morgan and G. W. Watson, *Physical Review B*, 2009, **80**, 233102.

25 J. Heyd, G. E. Scuseria and M. Ernzerhof, *The Journal of Chemical Physics*, 2006, **124**, 219906–219901.

26 A. Janotti, J. B. Varley, P. Rinke, N. Umezawa, G. Kresse and C. G. Van de Walle, *Physical Review B*, 2010, **81**, 085212.

27 P. Deák, B. Aradi and T. Frauenheim, *Physical Review B*, 2012, **86**, 195206.

28 E. Finazzi, C. Di Valentin and G. Pacchioni, *The Journal of Physical Chemistry C*, 2009, **113**, 3382–3385.

29 P. Deák, B. Aradi and T. Frauenheim, *Phys. Rev. B*, 2015, **92**, 045204.

30 A. Malashevich, M. Jain and S. G. Louie, *Physical Review B*, 2014, **89**, 075205.

31 P. Deák, B. Aradi and T. Frauenheim, *Physical ReviewB*, 2011, **83**, 155207.

32 G. Kresse and J. Furthmüller, *Computational Materials Science*, 1996, **6**, 15–50.

33 P. E. Blöchl, *Physical Review B*, 1994, **50**, 17953–17979.

34 J. P. Perdew, K. Burke and M. Ernzerhof, *Physical Review Letters*, 1996, **77**, 3865–3868.

35 S. Lany and A. Zunger, *Physical ReviewB*, 2009, **80**, 085202.

36 J. K. Burdett, T. Hughbanks, G. J. Miller, J. W. Richardson and J. V. Smith, *Journal of the American Chemical Society*, 1987, **109**, 3639–3646.

37 M. Landmann, E. Rauls and W. G. Schmidt, *Journal of Physics: Con-*

View Article Online
DOI: 10.1039/C6CP05798E

densed Matter, 2012, **24**, 195503.
38 H. Tang, F. Lévy, H. Berger and P. E. Schmid, *Physical Review B*, 1995, **52**, 7771–7774.
39 G. Makov and M. C. Payne, *Physical Review B*, 1995, **51**, 4014–4022.
40 S. Lany and A. Zunger, *Physical Review B*, 2008, **78**, 235104.
41 H.-P. Komsa, T. T. Rantala and A. Pasquarello, *Physical Review B*, 2012, **86**, 045112.
42 B. Lee, C.-k. Lee, C. S. Hwang and S. Han, *Current Applied Physics*, 2011, **11**, S293–S296.
43 N. Umezawa and J. Ye, *Physical Chemistry Chemical Physics*, 2012, **14**, 5924–5934.
44 C. B. A. O. Kubaschewski and P. J. Spencer, *Materials Thermochemistry 6th Ed*, Pergamon Press, Oxford, 1993.
45 K. Reuter and M. Scheffler, *Physical Review B*, 2001, **65**, 035406.
46 H. Irie, Y. Watanabe and K. Hashimoto, *The Journal of Physical Chemistry B*, 2003, **107**, 5483–5486.
47 Y. Hirose, N. Yamada, S. Nakao, T. Hitosugi, T. Shimada and T. Hasegawa, *Physical Review B*, 2009, **79**, 165108.
48 M. Grundmann, *The physics of semiconductors: an introduction including devices and nanophysics*, Springer Science & Business Media, 2006.
49 Y.-X. Weng, Y.-Q. Wang, J. B. Asbury, H. N. Ghosh and T. Lian, *The Journal of Physical Chemistry B*, 2000, **104**, 93–104.
50 P. Erhart, A. Klein and K. Albe, *Physical Review B*, 2005, **72**, 085213.
51 H. Chen and J. A. Dawson, *Phys. Rev. Applied*, 2015, **3**, 064011.
52 A. Weibel, R. Bouchet and P. Knauth, *Solid State Ionics*, 2006, **177**, 229 – 236.
53 S. Livraghi, M. Chiesa, M. C. Paganini and E. Giamello, *The Journal of Physical Chemistry C*, 2011, **115**, 25413–25421.
54 S. E. Taylor and F. Bruneval, *Physical Review B*, 2011, **84**, 075155.
55 I. Dabo, B. Kozinsky, N. E. Singh-Miller and N. Marzari, *Physical Review B*, 2008, **77**, 115139.
56 S. Lany and A. Zunger, *Physical Review B*, 2010, **81**, 113201.
57 A. G. Thomas, W. R. Flavell, A. K. Mallick, A. R. Kumarasinghe, D. Tsoutsou, N. Khan, C. Chatwin, S. Rayner, G. C. Smith, R. L. Stockbauer, S. Warren, T. K. Johal, S. Patel, D. Holland, A. Taleb and F. Wiame, *Physical Review B*, 2007, **75**, 035105.
58 T. Sekiya, K. Ichimura, M. Igarashi and S. Kurita, *Journal of Physics and Chemistry of Solids*, 2000, **61**, 1237–1242.
59 T. Sekiya, T. Yagisawa, N. Kamiya, D. Das Mulmi, S. Kurita, Y. Murakami and T. Kodaira, *Journal of the Physical Society of Japan*, 2004, **73**, 703–710.